




Development of PVA/GO Nanocomposites Membranes for Air-Filtration and Purification

Elham F. Mohamed¹ · F. Mohamed² · Asmaa El-Mekawy¹ · W. El Hotaby² 

Received: 11 September 2022 / Accepted: 8 June 2023 / Published online: 28 June 2023
© The Author(s) 2023

Abstract

Climate change due to the air pollution is actually one of the largest environmental challenges worldwide. Preparation and development of stable and highly efficient nanocomposite membranes remain a significant goal because of its enormous importance of controlling the environment. This study investigated a simple synthesis of poly (vinyl alcohol)/graphene oxide (PVA/GO) nanocomposite membrane for air pollutant remediation. The chemical and physical structures, morphologies, and conductivities were investigated as a function of the GO loading. The objective of the present study was to evaluate the efficiency of novel PVA/GO membranes in the removal of both formaldehyde (FA) as a pollutant VOCs model and SO₂ as a model of greenhouse gases. Furthermore, the purpose of this study is to identify good predictors for selecting the appropriate optimal GO content in GO/PVA nanocomposites that exhibit higher air pollutant removal performance as well as design an economical GO/PVA nanocomposite air purification system for removal of the air pollutants in the field. To our knowledge, field application of GO/PVA nanocomposite volatile organic compound (VOCS) filters and control of SO₂ gas pollutants from indoor air has not yet been realized. The nanocomposite membranes with an optimum GO content exhibited higher removal performance for the FA gas pollutant, this enhancement reached 90% in the laboratory scale. However, during the application in the field, it showed 75% FA removed from the indoor air. These new nano-membranes reveal also wide efficiencies of SO₂ removal (80%) when applied in the field. Therefore, this filter system proved an excellent efficacy in the removal of air pollutants and could be more promising in various industrial applications.

Keywords PVA · GO nano-membranes · Indoor air pollutants · Formaldehyde · SO₂ · Pollution control

1 Introduction

Air pollution and climate change are strongly related. The current challenge is air pollution, regarding not only of its effect on climate change but also its influence on human health, mortality and morbidity. Air pollutants include the air particles, toxic gases, and volatile organic compounds (VOCs). These pollutants affect the health of human and have destruction impacts to the environment, which contribute to the global warming. Indoor air pollutants are a very grave problem since the indoor air is usually 2 to 5 times more polluted than the outdoors. Nowadays, the people spend up to 80% of their time being at home. Hence, the quality of indoor air requires much more attention. Formaldehyde (FA) is a main pollutant of indoor air, which is principally liberated from the furnishing materials and building [1, 2]. Long-term exposure to FA may provoke severe health problems, such as respiratory diseases, cancer, and an irritation of the skin [3–5]. Due to the advanced industrial

✉ W. El Hotaby
Walid.mosad@gmail.com

Elham F. Mohamed
Elham_Farouk0000@yahoo.com

F. Mohamed
F_nrc@yahoo.com

Asmaa El-Mekawy
Asmaamekawy75@gmail.com

¹ Air Pollution Department, Environment and Climate Change Research Institute, National Research Centre, 33 EL Buhouth St., Dokki, Cairo P.O.12622, Egypt

² Spectroscopy Department, Physics Research Institute, National Research Centre, 33 ELBuhouth St., Dokki, Giza 12622, Egypt

powers, inorganic gaseous pollutants have been increasingly emitted over the recent decades and have become one of the major challenges of the modern societies.

Sulfur dioxide (SO₂) has been widespread emitted into the atmosphere from the fossil fuel burning in the industry; recently it has become the main challenge owing to its negative impact on the environment and human beings [6, 7]. Therefore, control its exposure in both industrial and a residential environment is essential. The Governments have put international goals to regulate the climate change, decrease the air pollutants and to improve the quality of air. Indeed, rising concerns about the quality of the air have led to developing a new ecological technology and materials. Recently, to reduce, eliminate and to solve the problems of air pollution, numbers of chemical, physical and biological techniques have been created to remediate successfully the pollutants [8–12]. Among the diverse, convenient technologies, the adsorption is broadly utilized and considered as an easy and simple method and it can efficiently eliminate various types of pollutants from the air [13–16].

Traditional adsorbents like the activated carbons (ACs) have been broadly utilized for pollutant control attributed to the implementation easiness. However, these adsorbents, especially ACs are not efficient to sufficiently remove certain VOCs types with a lower molecular weight like FA [17, 18]. Creation of practical and effective new adsorbents from carbon-based materials has recently been augmented. In recent years, a significant attention has paid to graphite-based materials such as graphene, graphene oxide (GO), and reduced graphene oxide (rGO) as additives in water purification membranes [19, 20]. They are ease of fabrication, chemically ease to functionalization, and have high mechanical strength. Among them, a single-layer GO is a two-dimensional (2D) atom-thick material that has demonstrated a great potential for water separation membranes. In particular, GO nano-sheets contain surface groups and edges such as oxygen moieties (carboxyl, –COOH, epoxy, –O–, and hydroxyl, –OH groups) that can be invested in fabricating nanocomposite membranes with excellent properties such as high chemical stability, high hydrophilicity, and antibacterial properties. The application of functional graphene as an adsorbent for air pollutants has been proposed. However, most studies have concentrated on the NH₃ adsorption by using GO and metal oxides modified composites. Few studies have also examined the removal of sulfur compounds and VOCs via adsorption.

GO nanocomposites were previously fabricated as GO/PVA membranes, but a new approach is to select a suitable optimal GO content in GO/PVA nanocomposites that exhibits higher air pollutant removal performance and development of an effective and economical GO/PVA nanocomposite air purification system in the field. To our knowledge, the application of GO/PVA nanocomposite filters for controlling

VOC and SO₂ gas pollutants from indoor air has not yet been realized. Additionally, the new filter can be seen as a green system: by using a small amount of GO in the PVA membrane and improving the efficiency of the pollutant removal filter device, the filter determines the key points of growth management and work, and has an economical design with less energy consumption. It increases filter equity and ultimately reduces exposure to indoor air pollutants by maintaining filter performance [21–23]

The present study aims to investigate the preparation of new PVA/GO nanocomposite membranes by simple techniques, to fully characterize the nano-membrane samples, and finally, to study the removal efficiency of these novel PVA/GO nano-membranes for formaldehyde (as a pollutant model of VOCs) and SO₂ (as a model of greenhouse gases) airborne pollutants in the laboratory scale and field.

2 Experimental Details

2.1 Preparation of PVA/GO Nanocomposite Films

The graphene oxide (GO) nano-sheets were prepared based on our previous work [24, 25], as a modified Hummer's method was utilized. A clear solution of 1% w/v PVA polymer was obtained using Milli Q deionized water with continuous mechanical stirring at 1000 rpm. Then, the desired amount of GO nano-sheets were suspended in 10 ml of deionized water using a Tip sonicator for 10 min then added drop by drop to the polymer solution with continues stirring in order to obtain a homogenous mixture. The obtained polymer/GO solution was sonicated for 20 min to get a fine dispersion. The PVA and PVA/GO solutions of same volume were casted in polypropylene dishes of the same diameter. The casted solution was inserted in a hot air oven kept at 60 °C for 3 days to dry, and a fine PVA/GO nanocomposite film was obtained. The PVA/GO nanocomposite films contain GO with concentrations 0 wt.%, 3 wt.%, 6 wt.%, 9 wt.%, 12 wt.%, and 15 wt.%, hereafter we labelled the samples with respect to their GO content as P0, P1, P2, P3, P4, and P5, respectively.

2.2 Lab Scale Screening Performance of the Prepared PVA/GO Nanocomposite Membranes: Formaldehyde Gas as a Pollutant Model

The removal performance of PVA/GO nanocomposite membranes was evaluated in the laboratory scale by the batch experiment of FA contaminated air mixture. The prepared membranes were kept in contact with FA gas at 25 °C for 73 h to reach a concentration of the equilibrium extent. Before starting the removal step, the inlet FA concentration

in the gaseous phase was determined to be 100 ppm. This initial concentration was selected because many recent studies investigated that the exposure to high doses (> 100 ppm) of FA vapor can provoke salivation, cramps, vomiting, and death of the tested animals. Sampling and measurement of FA concentrations were performed by a colorimetric technique (Spectrophotometer, PerkinElmer) reported by the National Institute for Occupational Safety and Health (NIOSH) Method 3500 [20].

2.3 Application of the New PVA/GO Nanocomposite Membranes in the Field for Indoor Air Control

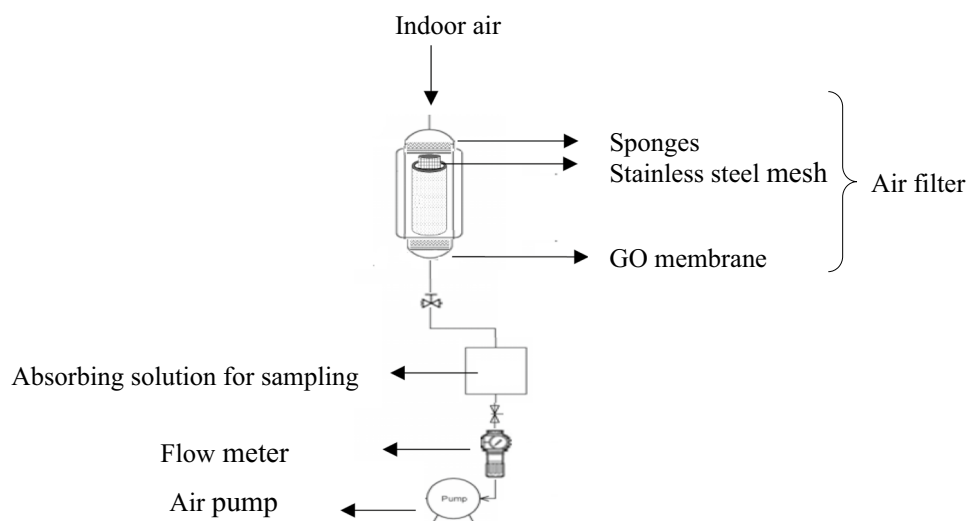
Figure 1 shows the schematic diagram of the filter system designed for this study. To investigate the removal of FA and SO_2 gas pollutants from the indoor air in the field by the prepared GO membranes, a cylinder-type column filter (8 cm internal diameter \times 12 cm height) was constructed. A stream of indoor air passes from the top of the filter by an air pump, which operated at a fixed flow rate of 2 L min^{-1} using an air flow meter at the atmospheric pressure and ambient temperature (25°C). The central section of the new filter is a stainless-steel cylindrical mesh with a diameter smaller than that of the principal frame, thus this design allows passing the air via the filter for treatment. The GO membrane material is steady over the central cylinder; a sponge was utilized in both side portions (top and bottom) of the filter that helps to keep the efficiency, extends the filter life, and prevents the dust to pass and block the filter sites. The performance of this new filter was investigated for the removal of FA and SO_2 pollutant gases from the indoor air. Prior to starting the experiment, a blank experiment was performed using the same designed filter system with PVA membrane/zero GO system to evaluate the removal capacity of the sponge and PVA membrane. The blank system has no removal efficiency

for both FA and SO_2 pollutants. The air samples were then collected over 3 days through the empty designed reactor system for determining the initial FA and SO_2 gas concentrations in the indoor air. Samples were collected during the experiment time by withdrawing air with a constant flow rate (2 L min^{-1} , for 72 h) via a bubbler with a volume of 100 mL involving the gas absorbent solution. The air samples were collected and analyzed with and without using the new GO membranes according to the previous reports using an Ultraviolet/Visible (UV/VIS) spectrophotometer (NOVASPEC 4049 Spectrophotometer LKB BIOCHROM)[26, 27]. The new GO membrane system was utilized to evaluate and control FA and SO_2 for 3 consecutive days.

2.4 Characterization

For the FT-IR analysis, a Bruker Optics Vertex 80 FT-IR spectrometer (Germany) in the reflection mode of the attenuated total reflection unit (ATR-diamond crystal) is used. Raman spectra were recorded using confocal Raman Microscope, WiTec alpha 300R-Germany, with an excitation laser source of 532 nm and power of 5mW. The crystallographic features of the PVA/GO nanocomposites were conducted by means of the X-ray diffraction (XRD) traces in reflection mode with PANalytical X'pert, Netherlands using CuK_α line ($\lambda = 1.540 \text{ \AA}$) source in the diffraction 2θ angular range $10\text{--}80$. The absorbance of nanocomposite membranes was conducted in the wavelength range $190\text{--}2500 \text{ nm}$ utilizing a double beam spectrophotometer (SP, V-570, JASCO, Japan). For electrical measurements, the PVA or PVA/GO sheets were sandwiched between two electrodes in Alpha-A Analyzer-Technologies GmbH & Co. KG. The measurements were achieved in the frequency range of $\nu = 10^{-1}$ to 10^7 Hz and at room temperature. The surface image morphology and stoichiometry of polymer nanocomposites were

Fig. 1 Schematic diagram of the air filter system designed using new PVA/GO nanocomposite membranes for this study



achieved by field emission scanning electron microscope which is attached with energy dispersive X-ray (FESEM, Quanta 250 FEG, USA).

3 Results and Discussion

3.1 FTIR Analysis

The functionalization and interaction of GO with PVA polymers were examined by FT-IR analysis displayed in Fig. 2a. The spectrum of the pure PVA exhibits bands at 3300 cm^{-1} , 2900 cm^{-1} , 1730 cm^{-1} , 1256 cm^{-1} and 1090 cm^{-1} , which are assigned to O–H, C–H, C=O stretching vibrations, C–H bending, and C–O stretching, respectively [28]. Loading the PVA matrix with GO slightly alters the spectra; few changes can be recorded. For instance, the intensity of the whole spectral bands is diminished. Regarding the band revealing the O–H stretching vibration, it is slightly downshifted and broadens. These findings may be attributed to a degradation in the hydrogen bonding among the hydroxyl groups in PVA chains and

instead, it suggested that GO canceled the hydrogen bonding among the PVA chains by inserting another way of interaction as the oxygen functional groups of GO and the hydroxyl groups on the polymer can do [29–31].

3.2 Raman Analysis

The Raman spectra of pure PVA and PVA/GO nanocomposite membranes are shown in Fig. 2a. The Raman spectra of pure PVA exhibits the bands corresponded to stretching and deformation vibrations of C–H and O–H group vibrations at 2913 , 1440 cm^{-1} , and 1137 cm^{-1} respectively [30–32]. In the case of GO, it is well known that two main bands are expected in the Raman spectrum; the G band at 1600 cm^{-1} and the D band at 1332 cm^{-1} . The G band demonstrates the C–C bond stretching vibration of graphite materials, while the D band ascribed to structural disorder or defects in graphene nanolayers [30–32]. It is also expected to observe a band at a doubling of the frequency of the D band (at 2656 cm^{-1}) as so-called 2D band, describing a second-order two phonon [33].

Here, in the GO/PVA nanocomposites spectra, the 2D band disappeared. This is due to the presence of the oxygenated functional groups on the surface of the GO like the carboxyl functional groups; they adhere well with PVA matrix along the hydroxyl groups [34]. There is a change in the shape and intensity of D and G bands in the composites with the increase of GO content. This may be due to the change in the elastic constant of the harmonic oscillator, containing GO/PVA, which is related to the charge transfer between the GO and PVA [30]. The broadening of the PVA peak in the nanocomposites with increasing GO content can be attributed to the association of GO and PVA matrix with hydrogen bonding formation [30].

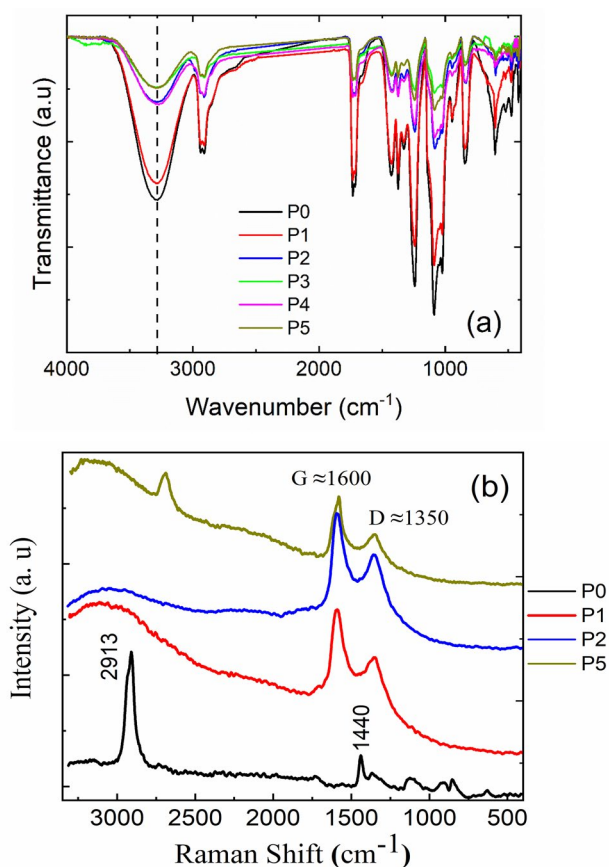


Fig. 2 a FTIR spectra and b Raman spectra of the PVA and PVA loaded with GO at different concentrations

3.3 X-Ray Diffraction Analysis

The XRD spectrum of PVA/GO nanocomposite for different concentrations of GO loading is illustrated in Fig. 3. For pure PVA, a characteristic peak at 19.68° is observed, which is attributed to the crystalline phase of the PVA polymer of (101) plan [35]. When the PVA is loaded with GO, the XRD pattern of the sample contains a higher concentration of GO is similar to that of the PVA as no additional peaks for GO is seen. Yet, the intensity of the (101) peak is increased. This suggests that the GO fillers do some changes in the crystalline phase of the PVA matrix. Also, this indicates that the GO nanofillers are well dispersed in the PVA matrix at the molecular phase.

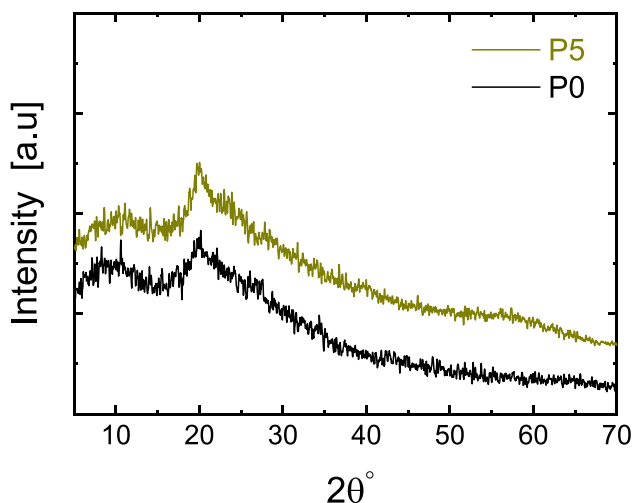


Fig. 3 XRD diffraction pattern of samples: neat PVA (P0) and that loaded with higher concentrations of GO (P5)

3.4 Morphological Structure and EDS Analysis

Scanning electron microscopy (SEM) used to study the surface morphology for PVA/GO before and after testing

as air filters as shown in Fig. 4. The micrographs of PVA/GO before exposing to the contaminant (Fig. 4a) revealed smooth well dispersed GO particles in the polymeric matrix without any grooves or aggregations. While Fig. 4b, which represents PVA/GO film after removal of contaminant shows adequate changes in the morphological structure due to the interaction with contaminants and the EDS analysis confirms the presence of sulfur ions in the polymeric matrix.

3.5 Optical Analysis

Identifying the optical properties and possible electronic transitions inside PVA/GO nanocomposite membranes can be acquired via UV–Vis spectroscopy. Figure 5a presents the absorption spectrum for PVA /GO membranes at different concentrations in the range from 190 to 2500 nm of wavelength.

For the pure PVA, the spectra exhibited a band located about 270 nm which can be ascribed to π - π^* electronic transition of the carbonyl group of PVA (C=O)[36–38]. Upon filling with GO, the absorption enhances and hence the transparency decreases. The position of the peaks for all amounts of GO filler to the PVA shifts towards red wavelengths, which may give an indication of the decrement of

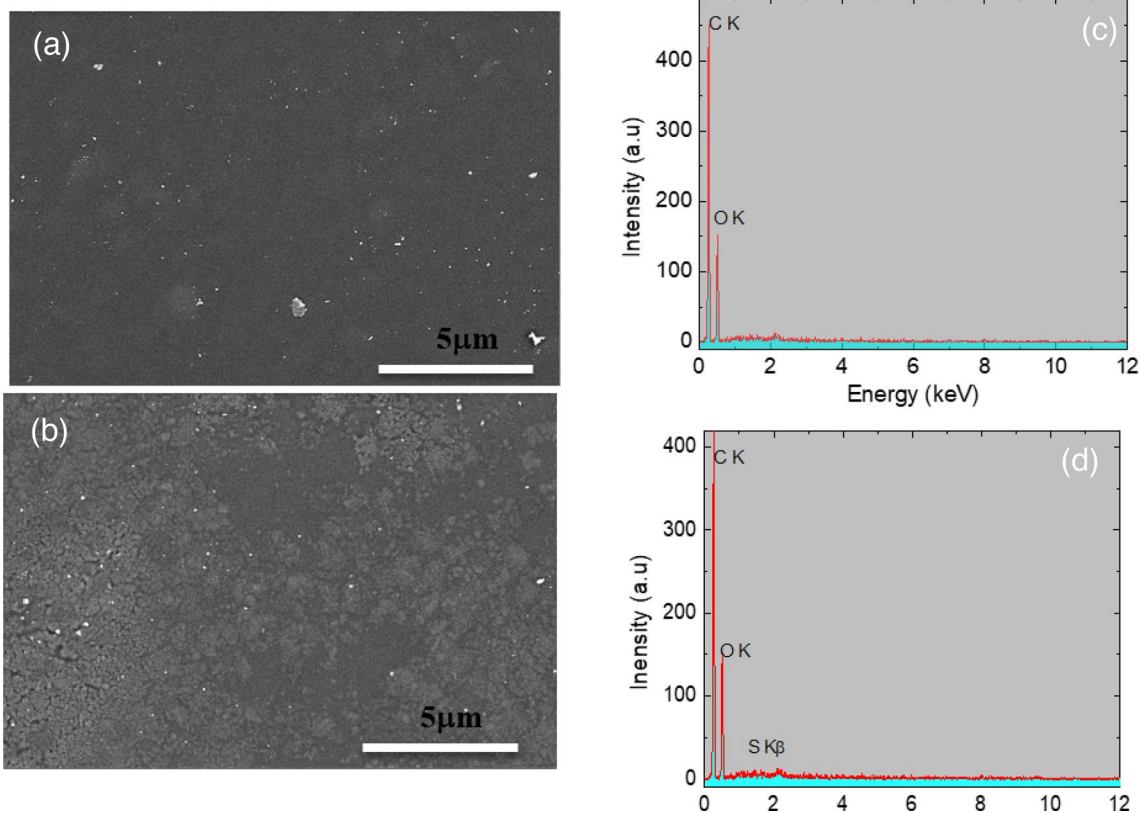


Fig. 4 SEM images of the surfaces of **a** PVA/GO nanocomposite with higher concentration (P5) before using as filter and **b** after using as filter; note their relevant EDS spectra are **c** and **d**, respectively

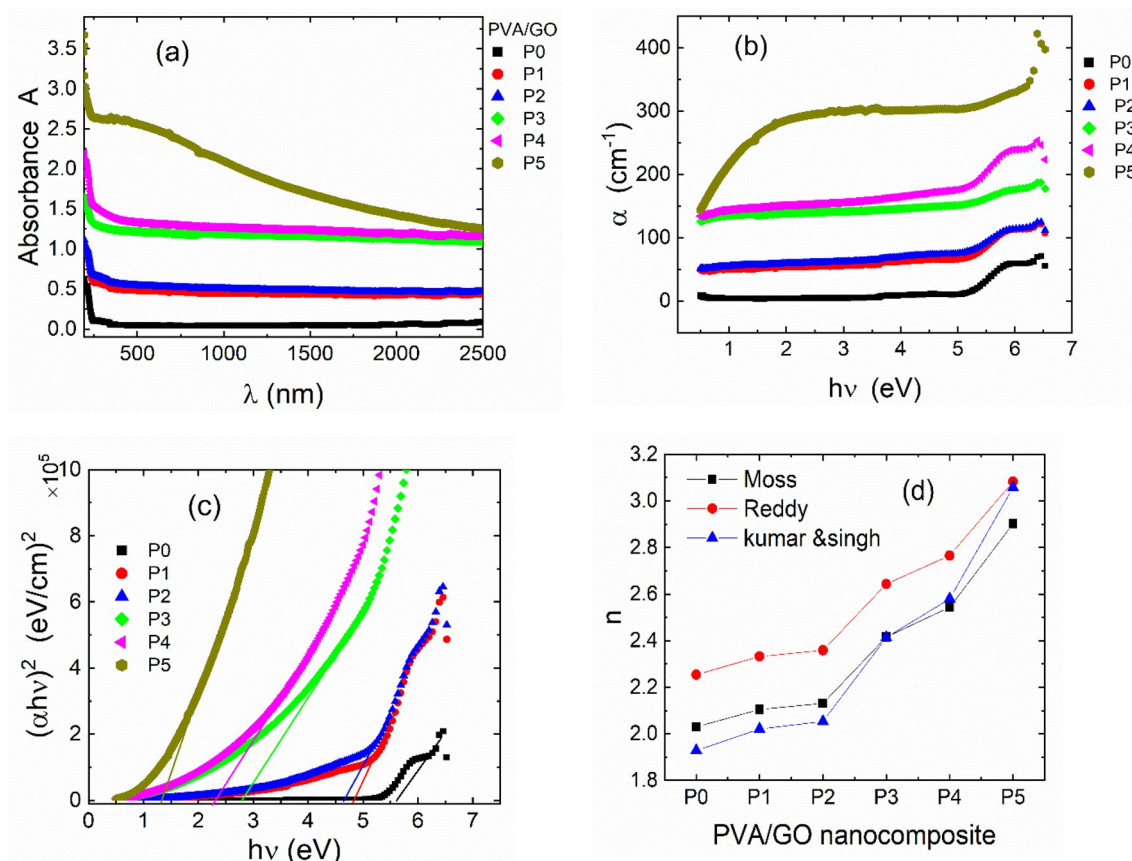


Fig. 5 **a** The absorbance as a function of wavelength; **b** and the absorption coefficient (α), and $(\alpha h\nu)^2$ as a function photon energy ($h\nu$) for various concentrations of PVA /GO, respectively. **d** The sample dependence of refractive index (n) by different models

the band gap energy. In the absorption coefficient (α) representation versus incident energy ($h\nu$) as illustrated in Fig. 5b, this shift can be inspected better, where α is computed from Eq. 1.

$$\alpha = \frac{2.303}{d} A(\nu) = \frac{2.303}{d} \log \left(\frac{I_o}{I} \right) \quad (1)$$

here I_o and I are the intensity of both incident and transmitted light, respectively, while A and d define the absorbance, and t film thickness, respectively.

The absorption coefficient (α) is related to the optical band gap (E_g) via Tauc's relation [39]:

$$\alpha(E) = \beta(E - E_g)^\gamma \quad (2)$$

β is an energy-independent constant and E denotes the energy of incident photons and γ defines the index of the nature of transition ($= 1/2, 3/2$ for direct transition, and 2 and 3 for indirect transition based on whether they are allowed or forbidden, respectively). To determine the band gap energy (E_g), plots of $(\alpha h\nu)^2$ as a function of photon energy is represented in Fig. 5c. The E_g of PVA is 5.55 eV which is well

consistent with previously reported data [40]. For all samples, the E_g values decrease steeply with the incorporation of GO from 5.55 to 4.8, 4.6, 2.67, 2.4, and 1.32 eV, respectively. The reduction of the band gap energy may happen as a result of forming of new energy levels in the space charge area and/or refer to the increase of the localized states [41].

For the fabrication and design of any optoelectronic or related devices, knowing the relation between the refractive index (n) and the band gap energy (E_g) is necessary. Some models have been imposed to find a proper relation, e.g., Moss[42], Kumar and Singh [43], and Reddy[44] as the following relations:

$$\text{Moss } n = \sqrt[4]{95/E_g} = 3.12 \sqrt[4]{E_g} \quad (3)$$

$$\text{Kumar and Singh, } k = 3.3668, c = -0.3224 \quad (4)$$

$$\text{Reddy } n = \sqrt{12.417/(E_g - 0.365)} \quad (5)$$

The obtained values of the refractive index n using these models are plotted as a sample function and depicted in Fig. 5d. While the band gap decreases with increasing GO content, the refractive index increases with increasing GO.

3.6 Electrical Properties

The dielectric permittivity ϵ' of pure PVA and those loaded with different concentrations of GO measured at 30 °C are illustrated in Fig. 6a. It is obvious that, the values of ϵ' enhance with increasing GO. It is clear that the ϵ' highly increases at low frequencies, which refers to the electrode polarization effects.

The dielectric permittivity ϵ' of pure PVA and those loaded with different concentration of GO measured at 30 °C are illustrated in Fig. 6a. It is obvious that, the values of ϵ' enhances with increasing GO. It is clear that the ϵ' highly increases at low frequencies which refers to the electrode polarization effects.

Upon incorporation of GO in the PVA matrix, an additional interfacial polarization effects are expected to arise up [45, 46]. In a system of multicomponent, interfacial polarization is aroused as a building physical barrier, which impedes the charge, which was observed by other [47]. Figure 6b shows the frequency dependence of the conductivity σ' of PVA/GO nanocomposite membranes. The conductivity increases with frequency, which changes from power-law dependence to the other; it is almost frequency independent exhibits (a plateau like) at low frequency. It follows the power law relation $\sigma = A(1 + \omega^b)$, ω defines the angular frequency, A is a frequency independent parameter and b is a power law exponent. The $b \leq 1$ values are existed, i.e., an electronic hopping process governs the conduction mechanism [48]. It is also visualized that the conductivity boosts upon filling with GO. Such enhancement may be

due to setting up more conduction paths connecting the GO particles.

3.7 Screening of the Removal Performance of the Development of PVA/GO Nanocomposite Membranes

To test the removal potential of the prepared GO nano-membranes, a lab experiment was conducted using high FA concentration (100 ppm). The prepared membranes were kept in contact with FA gas at 25 °C for 72 h to attain an equilibrium level. The efficiency of the prepared GO membranes was examined as represented in Fig. 7. In this scaled-up using high inlet FA concentration (100 ppm), the obtained results were even better where all prepared GO membranes revealed a considerable removal capacity of FA gas pollutant. The membrane efficiency via FA removal from the gaseous phase was in the following order: P5 > P4 > P3 > P2. This trend

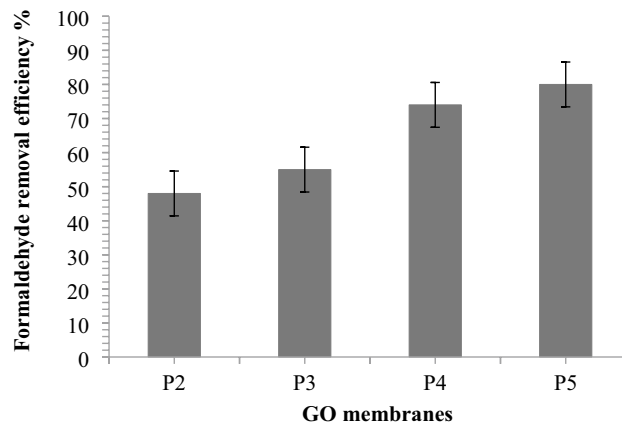


Fig. 7 Lab scale screening performance of the prepared GO nano-membranes for formaldehyde gas removal

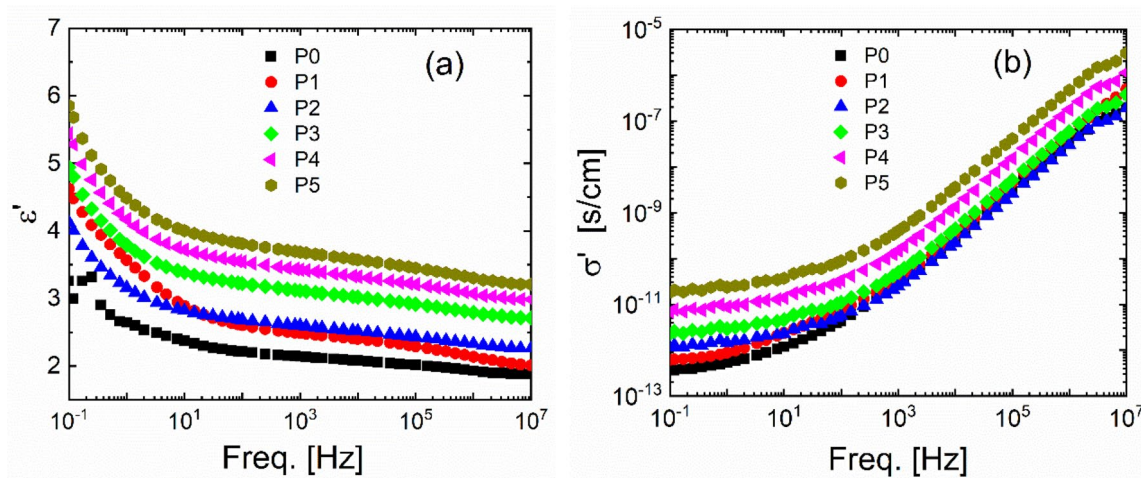


Fig. 6 Dielectric permittivity ϵ' (a) and real part of the conductivity σ' (b) of PVA and PVA/GO nanocomposites at different concentrations

coincided with the required amounts of GO nano-sheets that were added to the homo-polymer mixture to form the prepared GO membranes. The removal efficiency of this system towards FA was 80% for P5, 74% for P4, 55% for P3, and 48% for P2 with a GO content of 2%, 3%, 7% and 12%, respectively. The FA adsorption did not proceed with a high performance when a small GO amount was used due to the limited number of GO adsorption sites. In certain regards, some adsorbents show a good efficiency in controlled conditions of initial target gas concentration at an unrealistic elevated level. These materials could proceed very poorly in the practical conditions when using a concentration is not as high as the experimental one and a competition with other pollutants in the field was carried out. To prevent such

challenge, the use of novel materials in the field is important to evaluate the adsorbent performance. In the next section, the novel GO nano-membranes were utilized with a real stream of indoor air to compare their performance.

3.8 Field Application of the New Development of PVA/GO Nanocomposite Membranes for Indoor Formaldehyde Pollutant Control

The performance of GO nanocomposite membranes for the FA removal is depicted in Fig. 8a. The inlet FA concentrations during the treatment period were not constant and varied during this period, this can be explained by the fact that FA and other pollutants such as SO₂ gas depend

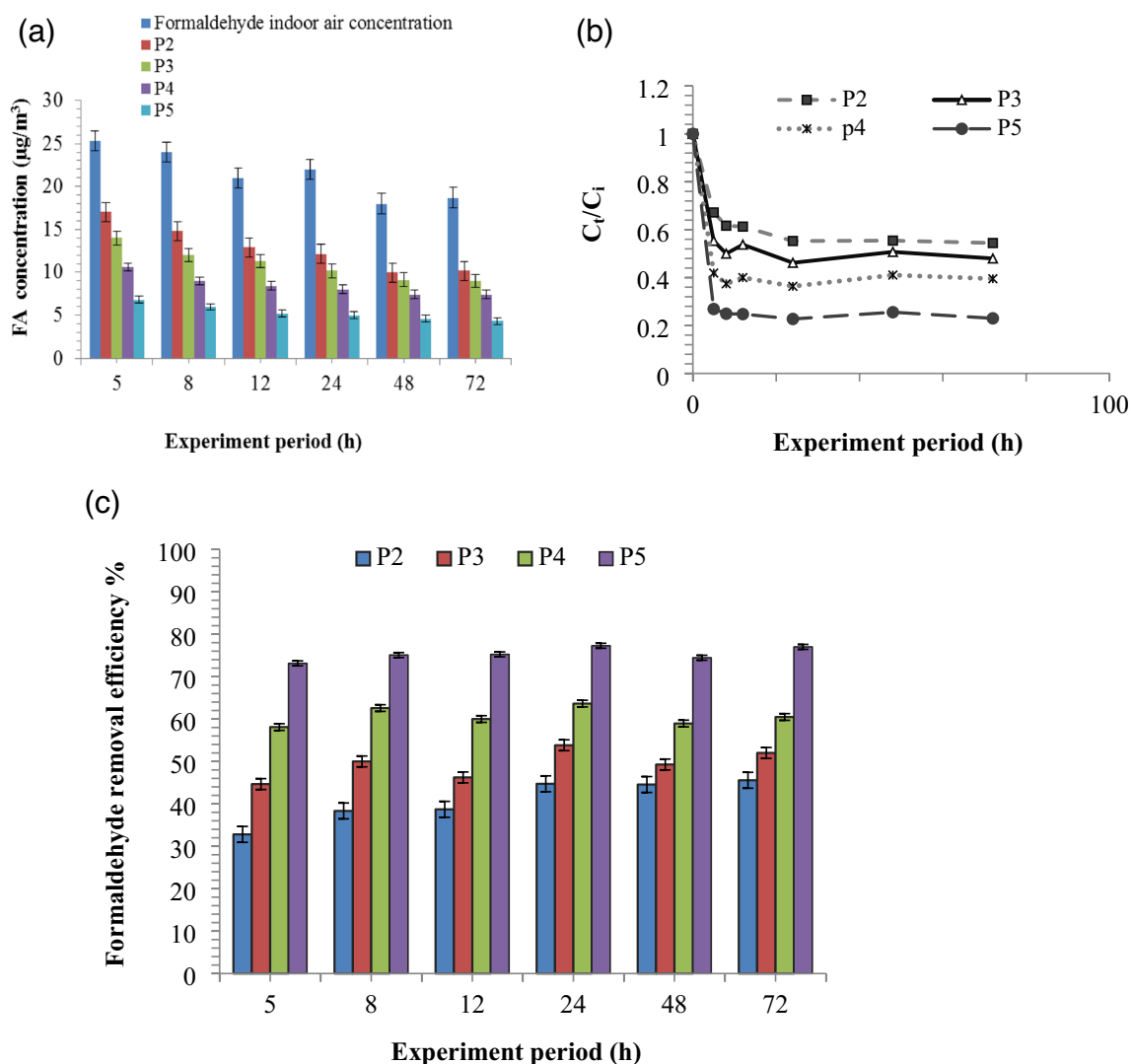


Fig. 8 **a** Formaldehyde concentration in the indoor air before (blue) and after using the new GO nanocomposite membranes (P2–P5), **b** average concentrations of formaldehyde gas removal from the indoor air during a treatment period of 80 h using the new prepared PVA/GO

nanomaterial membranes (P2–P5), and **c** formaldehyde removal efficiency from the indoor air during the treatment period using the new prepared PVA/GO nanomaterial membranes (P2–P5)

on the activities of humans. The findings indicated that upon passing indoor FA gas through all prepared GO membrane filters, FA rapidly decreased due to its adsorption onto the GO membranes. However, among all filters, the indoor FA removal efficacy was the highest with P5 membrane filter, while becoming less significant as the loading amount of GO over the membranes decreased in the order of $P5 > P4 > P3 > P2$.

It was found that the FA concentration in the inlet indoor air greatly decreased and reached $6.8 \mu\text{g m}^{-3}$, which represent nearly $\frac{1}{4}$ of the initial concentration ($25 \mu\text{g m}^{-3}$) within the first 5 h of treatment. In the second exposure period (8 h), the FA concentration values in the treated air after passing through P5 membrane and the untreated inlet air samples were decreased from 24 to $5.8 \mu\text{g m}^{-3}$, approximately the same of the first 5 h treated period. After 12 h and 24 h of the treatment using P5, the results showed that the FA concentrations in both samples were decreased from ~ 22 to $\sim 5 \mu\text{g m}^{-3}$. The additional application of P5 filter in the second and third day (after 48 h and 72 h) indicated that the P5 membrane is still able to remove extra pollutants and FA gas concentration decreased from ~ 14 to $\sim 4 \mu\text{g m}^{-3}$. The FA adsorption via GO filters could be probably performed by both physisorption and chemical adsorption [49]. Moreover, the high porosity and specific surface area of GO promoted the physical capture of FA molecules. The prepared GO samples involved also several oxygen containing functional groups. The FT-IR spectrum exhibited a broad peak and high-frequency area around 3200 cm^{-1} and 1735 cm^{-1} , which were attributed to both the O–H stretching mode and C=O, indicating the presence of –COOH group on the GO surface (Fig. 2). Likewise, the –OH and –COOH groups of GO may react with the FA pollutant in the indoor air. It should be pointed out that the most stable adsorption structure of the FA is when it interacts with the O atoms of GO surface via its H atom to form H-bonds [49, 50]. In addition, various studies cited that the polar VOCs usually prefer to interact with the polar materials, like the surface of GO. Hence, GO can easily go an interaction with VOCs towards polar functional groups present on the GO surface [51–53]. Because FA is a polar compound and GO exhibits strong hydrophilic characters due to the oxygen containing groups, the polar FA was efficiently adsorbed by the new prepared GO nano-membranes.

Figure 8b shows the performance of the new PVA/GO carbonaceous nanomaterial membranes, including the decrease in FA gas concentration during an experimental time of 80 h. Upon passing indoor air via the GO filter, the FA sharply decreased in the first stage for all GO nano-membranes used. Then the removal capacity was gradually decreased. The comparison between the adsorption performances of the prepared GO nanomaterial membrane samples showed that P5 membrane revealed the strongest adsorption

capacity towards the removal of FA gas among all prepared GO nano-membranes. Similarly, Esrafilı and Dinparast [49] reported that GO has an excellent adsorption capacity for FA.

The high removal efficacy can be explained on the basis of that Graphene has a large theoretical specific surface area and Graphene oxide has several oxygen-containing functional groups such as –OH, –COOH, and epoxides on its surface, indicating their potential for the adsorption processes. Generally, the most important GO characteristics of its layered configuration and negatively charged surfaces can play a significant role in adsorption. GO and its modified forms are good adsorbents for the removal of toxic gases. Their adsorption mode is varied from other carbons in which the porosity plays an efficient role in adsorption.

To study the system performance of the PVA/GO membrane filters, FA gas removal efficiency was calculated and represented in Fig. 8c. The performance of the GO nano-membranes showed that the P5 filter revealed a better performance than the other studied GO membranes. It was found that approximately 73%, 58%, 45%, and 33% of FA removal efficiency reached within 5 h of the treatment for P5, P4, P3 and P2, respectively. In the next exposure periods, the removal efficiency was slightly increased to reach its maximum values of 77%, 63%, 53%, and 45% for P5, P4, P3 and P2, respectively. It was assumed that the use of new prepared PVA/GO nanocomposite membranes led to enhance the adsorption performance. Similarly, Sun et al. [54] supposed that the composite formation with GO augmented the adsorption capacity of n-hexane by 93%. Generally, graphene-based materials enhance the surface and the forces of interaction with small molecules, like FA and ethanol, particularly when exist in composite forms, leading to a high adsorption capacity. In other reports, the higher surface area, porosity, and available oxygen containing functional groups of Cu-BTC@GO composite led to a high adsorption performance of ethanol (635 mg g^{-1}) [55]. Meanwhile, the existence of COOH and OH groups on the GO surface can increase the H-bonds and the forces of van der Waals during the VOCs adsorption [56]. Furthermore, the competing adsorption between VOCs and water vapor strongly affects the adsorption processes. Otherwise, the presence of oxygen-containing groups on the GO surface gives the composite high hydrophilic characters. In this sense, removing these groups generates more sp^2 carbon atoms on the adsorbent that would reduce the reaction between the water vapor and adsorbent; leading to an increase in the VOCs adsorption onto the GO based adsorbents [57]. It was assumed that various factors were capable of improving the efficiency of GO composites via VOCs removal, like (1) high surface area; (2) increased surface functional groups of the GO, which tends to augment the adsorption of the target pollutant on the composite surface, and (3) generating the polarity attributed

to the O-based functional groups, which facilitates the polar pollutant adsorption.

3.9 Field Application of the New Development of PVA/GO Nanocomposite Membranes for SO₂ Indoor Air Pollutant Control

Sulfur dioxide is one of the significant air pollutants in the management of gas waste due to the high temperature required for removing it. Owing to its high stability against corrosive gases, carbon-based adsorbents are favorably used for adsorbing SO₂. Indeed, the experimental conditions of temperature and pressure in which the adsorption process is taken place, having fundamental importance, not only in

terms of performance, but also in terms of costs. The current study developed new PVA/GO nanocomposite membrane filters that can remove SO₂ at room temperature. The performance of these filters for indoor SO₂ removal is represented in Fig. 9a. The results indicated the ability of all tested filter samples to adsorb the indoor SO₂ gas pollutant.

In general, GO samples have higher specific surface areas and folded arrays that could improve the pollutant adsorption by physisorption. However, the adsorption is a function of not only the porosity and geometry, but also the chemical constituents. Generally, the appropriate balance between surface area, hydrophobicity, and functional groups of GO nanocomposite membranes is an excellent concern for improving the adsorption of diverse toxic gases. It was

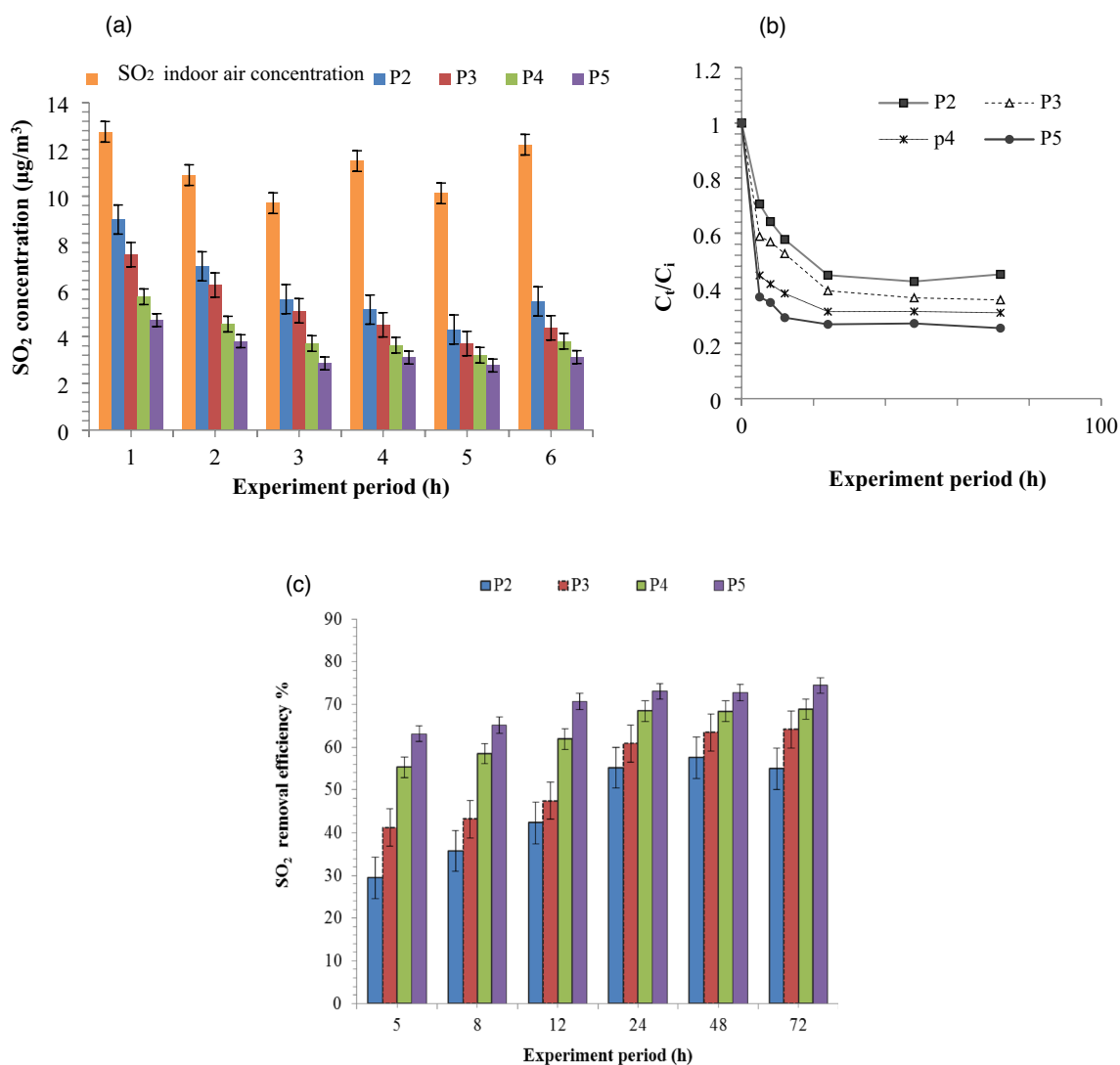


Fig. 9 **a** Sulfur dioxide concentration in the indoor air before (Orange) and after using the new PVA/GO nanocomposite membranes (P2–P5), **b** average concentrations of SO₂ gas removal during the experimental time of 80 h using the new prepared PVA/GO nano-

material membranes (P2–P5), and **c** sulfur dioxide removal efficiency from the indoor air during the treatment period using the new prepared PVA/GO nanomaterial membranes (P2–P5)

found that the removal performance was the highest with P5 membrane filter while it was less important as the loading quantity of GO over the PVA membrane decreased in the order of P5 > P4 > P3 > P2.

The results showed that the SO₂ concentration in the inlet indoor air decreased to reach more than the half (4.7 μg m⁻³) of the initial concentration (12 μg m⁻³) within the first 5 h of the treatment. During an exposure period of 8 h, the values of SO₂ in both the treated air after passing via P5 membrane and the untreated inlet indoor air (without filter) were decreased from 10.9 to 3.8 μg m⁻³. After 12 h of the treatment using P5, the SO₂ concentrations in both samples were reduced from ~10 to ~2.8 μg m⁻³. During a treating period of 24 h, more concentration of SO₂ gas decreased from 11.5 to 3 μg m⁻³, whereas, during the next two days (48 h and 72 h), the P5 membrane was still capable of removing more SO₂ gas pollutant and the SO₂ concentration was diminished to attain ~3 μg m⁻³.

Figure 9b shows the decrease in SO₂ gas concentration during the experimental time of 80 h using the prepared PVA/GO nanomaterial membranes. The performance of GO nanomaterial membranes showed the same trend of FA gas removal; this means that in the first stage, the SO₂ gas concentration in the indoor air rapidly decreased for all GO membranes used, and then the removal capacities gradually decreased until reached a constant mode. This higher SO₂ adsorption by GO samples at the beginning is presumed to be attributed to either the high concentration of oxygen based functional groups that are readily accessible to the pollutants as the air stream passed over the membranes or due to the high specific surface area of GO. With the continuous passing of the contaminated air, the GO active sites were saturated and led to no additional removal of pollutants. Among all the prepared membranes, P5 membrane revealed the strongest adsorption capacity for SO₂ gas pollutant. These results coincided with Yüksek et al. [58] who revealed the proficient performance of GO incorporated with PVA filters for the adsorption of SO₂ gas. Similarly, Babu et al. [59] studied the adsorption of SO₂ at lower pressure and noticed that GO bound SO₂ only by the physisorption process. The existence of O-based functional groups, particularly the C=O groups

augmented the SO₂ adsorption by GO composite membranes. Li et al. [60] observed also that the presence of C=O groups increased the SO₂ adsorption from a multi-component mixture containing SO₂, NO, chlorobenzene and H₂O vapors onto ACs. Understanding the role of various O-based groups on the GO surface, functionalities are the key to the capture accomplishment of SO₂. Several studies have pointed out that the role of oxygen containing groups is efficient on the SO₂ adsorption [61]. Yang et al. [62] cited that the -OH groups within the pores selectively fasten SO₂ by forming H-bonds that are strengthened by the weaker phenyl C-H...O=S=O links surrounding the pores.

The results depicted in Fig. 9c show the SO₂ gas removal efficiency using the prepared GO membranes. The performance test of the GO membrane filters shows that the P5 filter demonstrated a better performance than the other GO membranes. It was found that removal efficiencies of almost 63%, 55%, 40%, 29% of SO₂ for P5, P4, P3 and P2, respectively, were evaluated within 5 h of the treatment. In the next exposure periods, the efficiency of SO₂ removal was slightly elevated to reach 75%, 68%, 64%, and 55% for P5, P4, P3 and P2, respectively. Several reports investigated that GO and graphene based materials as well as their high surface areas are proficient factors in the adsorption of SO₂ and toxic gases [61–63]. The high surface area and the appropriate functionalities due to the O-based groups are the key to developing the prepared GO membranes for air pollutant adsorption. Moreover, the surface of GO enriched with negatively charged and layered structures plays also a significant role in the adsorption. Consequently, the new prepared PVA/GO nanocomposite membranes can attract as much attention as a proficient matrix for the adsorption of air pollutants, due to their characteristics, including high surface area, high functional groups, and high chemical and thermal stabilities.

As a comparison, Table 1 shows the amount of gaseous pollutants adsorbed on the prepared GO/PVA composites (present work) and previously reported amounts using various GO adsorbents. As can be seen, the pollutant adsorption capacity of the prepared GO materials is of the most significant value compared to that observed using other adsorbents (Table 1).

Table 1 Comparison of adsorption capacity of gaseous pollutants between prepared PVA/GO membranes and other studies

Adsorbents	Gaseous pollutants	Adsorption capacity (%)	References
PVA/GO	Formaldehyde (Lab. experiment)	90	Present work
PVA/GO	Formaldehyde (field experiment)	75	Present work
PVA/GO	SO ₂ (field experiment)	80	Present work
rGOMWKOH	Acetaldehyde	30	[64]
GO/MIL-101	Acetone	91.5	[65]
ZIF-8/GO	Toluene	87	[66]

Our innovations include investigating environmental viability assessments through governmental examination of filter removal efficiency, demonstrating higher performance in removing multiple air pollutants, and improving indoor air quality with different types of pollutants (VOCs and gases), including in field reuse to purify the air. Moreover, its durability and long-term benefits, as well as its simple design and economical creation of filters, have no negative impact on the environment. Additionally, according to environmental viability assessments, the design of PVA/GO nanocomposite membranes follows a recyclable product approach, making PVA a non-toxic and biodegradable material, making it an eco-friendly choice for several applications.

4 Conclusions

This study provides a development of PVA/GO nanocomposite membranes with new carbon materials, high surfaces, and various O-based groups. Such nanocomposite membranes could be utilized as adsorbents to effectively eliminate several pollutants, like FA and SO₂. Adsorption of the latter pollutants depends upon the amount, high surface area, and the functional groups of the GO membrane. It was concluded that the new prepared PVA/GO nanocomposite membranes resulted in the enhancement of pollutant adsorption efficiency. The performance of the GO membrane filters showed that the P5 filter was the best adsorbent for FA and SO₂ removal which shows 90% for formaldehyde in laboratories experiment while exhibits 75% removal in indoor experiments. Interestingly, the proposed new PVA/GO nanocomposite filter is a promising system for treating the indoor air containing various gaseous pollutants in the field; hence it can be applied in many industrial applications.

Acknowledgements The authors acknowledge the National Research Centre-Egypt for supporting, providing the infrastructure and research equipment to perform the study. In addition, we acknowledge the Science, Technology & Innovation Funding Authority (STDF) for financially supporting the open access agreement with springer nature.

Author Contributions All authors contributed to conception and design of the study. Material preparation, data collection, and analysis were performed by WME and FME. All Air treatment setup and calculations were performed by EFM and AE. The first draft of the manuscript was written by WME and all authors commented and contributed to subsequent versions of the manuscript. All authors read and approved the final manuscript.

Funding Open access funding provided by The Science, Technology & Innovation Funding Authority (STDF) in cooperation with The Egyptian Knowledge Bank (EKB). The authors declare that no funds, grants, or other supports were received during the preparation of this manuscript.

Data Availability The datasets generated during the current study are available from the corresponding author on reasonable request.

Declarations

Competing interests The authors declare that they have no competing interests.

Ethical Approval All authors agreed on the ethics approval.

Informed Consent All authors agreed on the consent to participate.

Consent for Publication Not applicable.

Open Access This article is licensed under a Creative Commons Attribution 4.0 International License, which permits use, sharing, adaptation, distribution and reproduction in any medium or format, as long as you give appropriate credit to the original author(s) and the source, provide a link to the Creative Commons licence, and indicate if changes were made. The images or other third party material in this article are included in the article's Creative Commons licence, unless indicated otherwise in a credit line to the material. If material is not included in the article's Creative Commons licence and your intended use is not permitted by statutory regulation or exceeds the permitted use, you will need to obtain permission directly from the copyright holder. To view a copy of this licence, visit <http://creativecommons.org/licenses/by/4.0/>.

References

1. J. Wang, Y. Tao, *Rec. Innov. Chem. Eng. (Formerly Recent Patents on Chemical Engineering)* **13**, 194 (2020)
2. E.F. Mohamed, M.A. El-Hashemy, N.M. Abdel-Latif, W.H. Shetaya, *J. Air Waste Manag. Assoc.* **65**, 1413 (2015)
3. K.H. Kim, S.A. Jahan, J.T. Lee, *J. Environ. Sci. Health C* **29**, 277 (2011)
4. J. Ma, Y. Sun, J. Yang, Z. Lin, Q. Huang, T. Ou, F. Yu, *Aerosol. Air Qual. Res.* **17**, 913 (2017)
5. F. Liu, X. Gao, M.A. Peng, F. Liu, X. Gao, M. Peng, *Separations* **9**, 31 (2022)
6. M. Mahmoodi Meimand, N. Javid, M. Malakootian, *Health Scope In Press*, (2019).
7. S.K. Sooriyan, N. Ibrahim, M.A. Hanif, M. Hasan, S. Abdullah, A.A. Adriansyah, B. Setianto, A. Syafiuddin, *Biointerface Res. Appl. Chem.* **12**, 7972 (2022)
8. G. Awad, E.F. Mohamed, *Appl. Catal. B* **253**, 88 (2019)
9. E.F. Mohamed, G. Awad, *Environ. Sci. Pollut. Res.* **27**, 24507 (2020)
10. E.F. Mohamed, G. Awad, *J. Ind. Eng. Chem.* **98**, 366 (2021)
11. E.F. Mohamed, G. Awad, *Adv. Powder Technol.* **32**, 2555 (2021)
12. E.F. Mohamed, G. Awad, C. Andriantsiferana, A.I. El-Diwany, *Environ. Technol.* **37**, 1197 (2016)
13. C. JulcourLebigue, C. Andriantsiferana, N'Guessan Krou, C. Ayrat, E. Mohamed, A.M. Wilhelm, H. Delmas, L. le Coq, C. Gerente, K.M. Smith, S. Pullket, G.D. Fowler, N.J.D. Graham, *J. Environ. Manag.* **91**, 2432 (2010)
14. E.F. Mohamed, C. Andriantsiferana, A.M. Wilhelm, H. Delmas, *Environ. Technol.* **32**, 1325 (2011)
15. H. Zaitan, E.F. Mohamed, H. Valdés, M. Nawdali, S. Rafqah, M.H. Manero, *Acta Chim. Slov* **63**, 798 (2016)
16. E.F. Mohamed, G. Awad, H. Zaitan, C. Andriantsiferana, M.H. Manero, *Environ. Technol.* **39**, 878 (2018)

17. S.C. Hu, Y.C. Chen, X.Z. Lin, A. Shiue, P.H. Huang, Y.C. Chen, S.M. Chang, C.H. Tseng, B. Zhou, *Environ. Sci. Pollut. Res.* **25**, 28525 (2018)
18. V. Kumar, S. Kumar, K.H. Kim, D.C.W. Tsang, S.S. Lee, *Environ. Res.* **168**, 336 (2019)
19. M.F. Elshahawy, G.A. Mahmoud, A.I. Raafat, A.E.H. Ali, E. Said, A. Soliman, *J. Inorg. Organomet. Polym. Mater.* **30**, 2720 (2020)
20. D. Rambabu, S.K. Sharma, M.A. Akbar, *J. Inorg. Organomet. Polym. Mater.* **2023**, 1 (2023)
21. J. Selvi, S. Mahalakshmi, V. Parthasarathy, *J. Inorg. Organomet. Polym. Mater.* **27**, 1918 (2017)
22. Y. Amaregouda, K. Kamanna, T. Gasti, *J. Inorg. Organomet. Polym. Mater.* **32**, 2040 (2022)
23. R.M. Moghazy, A.M. Bakr, S.T. El-Wakeel, W. El Hotaby, *Polym. Eng. Sci.* (2023)
24. M.A.K. Moharram, K. Tohami, W.M. el Hotaby, A.M. Bakr, *React. Funct. Polym.* **101**, 9 (2016)
25. A.M. Bakr, M.A. Moharram, K.M.T. Ereiba, W. el Hotaby, (n.d.)
26. (n.d.)
27. R. Harrison, R. Perry (1986).
28. M. M. H. El-Sayed, A. A. Mostafa, A. M. Gaafar, W. el Hotaby, E. M. A. Hamzawy, M. S. El-Okaily, and A. M. Gamal-Eldeen, *Biomedical Materials (Bristol)* **12**, (2017).
29. M. Cobos, M.J. Fernández, M.D. Fernández, *Nanomaterials* **8**, 1013 (2018).
30. M. Goumri, J.W. Venturini, A. Bakour, M. Khenfouch, M. Baitoul, *Appl. Phys. A* **122**, 1 (2016)
31. F. Mohamed, R.A. Zaghlool, W. el Hotaby, *J Mol Struct* **1250**, 131659 (2022)
32. I.Y. Prosanov, A.A. Matvienko, *Phys. Solid State* **52**, 2203 (2010)
33. J. Guo, L. Ren, R. Wang, C. Zhang, Y. Yang, T. Liu, *Composite B* **42**, 2130 (2011)
34. N. Lachman, C. Bartholome, P. Miaudet, M. Maugey, P. Poulin, H.D. Wagner, *J. Phys. Chem. C* **113**, 4751 (2009)
35. C.C. Yang, *Mater. Lett.* **58**, 33 (2004)
36. M.H. Abdel-Kader, M.B. Mohamed, *Appl. Phys. A* **126**, 1 (2020)
37. M. Mousa, Y. Dong, S.A. Khan, A. Rahman, F. Babiker, D.-A. Ibrahim, I. Vlaeva, T. Yovcheva, S. Sainov, V. Dragostinova, S. Stavrev, *J. Phys. Conf. Ser.* **253**, 012027 (2010)
38. K.S. Hemalatha, K. Rukmani, *RSC Adv.* **6**, 74354 (2016)
39. T.A. Hameed, W. Cao, E.M. Abdelrazek, I.K. el Zawawi, B.A. Mansour, H.E. Elsayed-Ali, *J. Mater. Sci. Mater. Electron.* **27**, 3209 (2016)
40. K. M. Abu Hurayra–Lizu, M. W. Bari, F. Gulshan, M.R. Islam, *Heliyon* **7**, (2021).
41. F. Mohamed, W. Sharmoukh, A.M. Youssef, T.A. Hameed, *Polym. Adv. Technol.* **33**, 1009 (2022)
42. H. Li, J. Yan, J. Zhou, et al., *Proc. Phys. Soc. Sect. A* **64**, 590 (1951)
43. S. Pal, R.K. Tiwari, D.C. Gupta, A.S. Verma, *J. Mater. Phys. Chem.* **2**, 20 (2014)
44. R.R. Reddy, K. RamaGopal, K. Narasimhulu, L.S.S. Reddy, K.R. Kumar, C.V.K. Reddy, S.N. Ahmed, *Opt. Mater. (Amst)* **31**, 209 (2008)
45. S. Ibrahim, A. Labeeb, A.F. Mabied, O. Soliman, A. Ward, S.L. Abd-El-Messieh, A.A. Abdelhakim, *Polym. Compos.* **38**, E147 (2017)
46. M.A. Saied, S.H. Mansour, A.A. Ward, I.S. Rahim, H.A. Zayed, K.N. Abdel Nour, *Polimery* **59**, 729 (2014)
47. N.N. Rozik, A.I. Khalaf, A.A. Ward, <https://doi.org/10.1177/1464420715581196> **230**, 526 (2015).
48. F. Mohamed, T.A. Hameed, A.M. Abdelghany, G. Turkey, *Polym. Bull.* **78**, 5205 (2021)
49. M.D. Esrafil, L. Dinparast, *J. Mol. Graph. Model.* **80**, 25 (2018)
50. K. Saito, Y. Hirabayashi, S. Yamanaka, *RSC Adv.* **11**, 32830 (2021)
51. J. Xu, J. Liu, S. Wu, Q.-H. Yang, P. Wang, *Opt. Express* **20**, 15474 (2012)
52. C. Bao, S. Bi, H. Zhang, J. Zhao, P. Wang, C.Y. Yue, J. Yang, *J. Mater. Chem. A* **4**, 9437 (2016)
53. V. Kumar, Y.S. Lee, J.W. Shin, K.H. Kim, D. Kukkar, D. Fai Tsang, *Environ. Int.* **135**, 105356 (2020)
54. X. Sun, Q. Xia, Z. Zhao, Y. Li, Z. Li, *Chem. Eng. J.* **239**, 226 (2014)
55. J. Yan, Y. Yu, J. Xiao, Y. Li, Z. Li, *Ind. Eng. Chem. Res.* **55**, 11767 (2016)
56. T.J.M. Fraga, M.N. Carvalho, M.G. Ghislandi, and M.A. da Motta Sobrinho, *Braz. J. Chem. Eng.* **36**, 1 (2019).
57. X. Zhang, B. Gao, A.E. Creamer, C. Cao, Y. Li, *J. Hazard Mater.* **338**, 102 (2017)
58. I. O. Yükses, O. Alptoğa, P. Altay, N. Karatepe, A. Onen, N. Ucar, *IOP. Conf. Ser. Mater. Sci. Eng.* **460**, (2018).
59. D.J. Babu, F.G. Kühl, S. Yadav, D. Markert, M. Bruns, M.J. Hampe, J.J. Schneider, *RSC Adv.* **6**, 36834 (2016)
60. Y. Li, Y. Guo, T. Zhu, S. Ding, *J. Environ. Sci.* **43**, 128 (2016)
61. D.J. Babu, D. Puthusseri, F.G. Kühl, S. Okeil, M. Bruns, M. Hampe, J.J. Schneider, *Beilstein J. Nanotechnol.* **9**(16), 1782 (2018)
62. S. Yang, J. Sun, A.J. Ramirez-Cuesta, S.K. Callear, W.I.F. David, D.P. Anderson, R. Newby, A.J. Blake, J.E. Parker, C.C. Tang, M. Schröder, *Nat. Chem.* **4**, 887 (2012)
63. A.C. Borges, M.H. Köhler, J.R. Bordin, *J. Nanomater.* **2019**, 9594816 (2019)
64. J.M. Kim, J.H. Kim, C.Y. Lee, D.W. Jerng, H.S. Ahn, *J Hazard Mater.* **344**, 458 (2018)
65. X. Zhou, W. Huang, J. Shi, Z. Zhao, Q. Xia, Y. Li, H. Wang, Z. Li, *J. Mater. Chem. A* **2**, 4722 (2014)
66. F. Chu, Y. Zheng, B. Wen, L. Zhou, J. Yan, Y. Chen, *RSC Adv.* **8**, 2426 (2018)

Publisher's Note Springer Nature remains neutral with regard to jurisdictional claims in published maps and institutional affiliations.